# Au Nanoparticles - Mesoporous $TiO_2$ Thin Films Composites as SERS Sensors: A Systematic Performance Analysis

M. Mercedes Zalduendo[a], Judith Langer[b], Juan J. Giner-Casares[b], Emilia B. Halac[c], Galo J. A. A. Soler-Illia[d], Luis M. Liz-Marzán[b,e], Paula C. Angelomé[a]*

(a) Gerencia Química, Centro Atómico Constituyentes, Comisión Nacional de Energía Atómica, CONICET, Av. Gral. Paz 1499, B1650KNA San Martín, Buenos Aires, Argentina.

(b) CIC biomaGUNE and CIBER-BBN, Paseo de Miramón 182, 20014 Donostia-San Sebastián, Spain.

(c) Departamento de Física de la Materia Condensada, Centro Atómico Constituyentes, Comisión Nacional de Energía Atómica, Av. Gral. Paz 1499, B1650KNA San Martín, Buenos Aires, Argentina.

(d) Instituto de Nanosistemas, UNSAM, CONICET, 25 de mayo 1021, 1650 San Martín, Buenos Aires, Argentina.

(e) Ikerbasque, Basque Foundation for Science, 48013 Bilbao, Spain

* Corresponding author email: angelome@cnea.gov.ar

**ABSTRACT**

The combination of plasmonic nanoparticles and mesoporous materials is of much interest in applications such as sensing or catalysis. The production of such hybrid materials can be done in various ways, leading to different architectures. We present a comparative study of the SERS performance of different nanocomposite architectures comprising mesoporous $TiO_2$ thin films and Au nanoparticles (NPs). The selection of $TiO_2$ as mesoporous support material was based on its high chemical and mechanical stability. Au NPs of different sizes and shapes were placed at different locations of the composite and used as a plasmonic material compatible with the synthesis conditions of the mesoporous films, displaying a high chemical stability. Using *p*-nitrothiophenol as a molecular probe, we evaluated the performance toward surface-enhanced Raman scattering (SERS) sensing, on the basis of minimum acquisition time, spot-to-spot reproducibility and limit of detection. The obtained results indicate that each platform features different sensing capabilities. While systems comprising Au NPs within the mesopores allow working with low acquisition times and present high signal uniformity, only a detection limit of μM was achieved. On the other hand, those systems made of branched Au NPs covered with mesoporous films require low acquisition times and can achieve detection limits as low as 10 pM, but signal uniformity is compromised. We propose that careful comparison of different SERS platforms based on Au NPs and mesoporous thin films will facilitate selecting an appropriate configuration for any desired application.

## INTRODUCTION

Surface-enhanced Raman scattering (SERS)[1-2] spectroscopy has become a technique of choice for potential application in trace-molecule detection. SERS exploits the amplification of the Raman signals of molecules located at, or very close to, the surface of metallic nanostructures supporting localized surface plasmon resonances (LSPRs).[3] As a spectroscopic technique, SERS provides vibrational information of the molecules under study, allowing specific detection that can be used to determine the presence of a given trace-level analyte,[3] even reaching the single molecule detection limit.[4-6] Consequently, SERS has been employed in the detection of molecules and ions with application in analytical chemistry,[3, 7] food science,[8] environmental sciences[9] and biomedicine,[10-11] just to mention a few. This technique can also be used to obtain information about structural and molecular conformations, to monitor changes as a function of time and to understand molecule-plasmonic surface interaction. Hence, SERS can also be used to understand biomedical processes,[12-16] to perform *in operando* studies[17] and for surface characterization.[18]

The enhancement of Raman scattering by plasmonic effects is largely determined by the properties of the amplifying platform. The main parameters behind this effect are related to the composition, size and morphology of the plasmonic nanostructures and their relative distribution within the support,[19-21] which determines the presence of so-called *hot spots*, i.e. regions in which the electromagnetic field is highly concentrated.[22] As a consequence, great effort has been devoted to the development of SERS substrates for specific applications.[23-26] Although much of the research has been so far focused on obtaining the highest possible signals, application to real analytical problems requires a balance of numerous factors, including ease and cost of preparation, ease of use, spot-to-spot and sample-to-sample reproducibility, among other critical issues.[20] The ideal composite for SERS should be easy to prepare and handle, robust, and chemically stable; and should also provide the highest possible signal, though sensitivity requirements may be very different for each specific application.[23, 27]

The original substrates for SERS were electrochemically roughened metal electrodes,[1] but shortly after metallic nanoparticles (NPs) were identified as an excellent alternative, being nowadays the most studied class of substrates. The simplest SERS experiments consist of mixing an analyte solution with a suspension of metal NPs (mainly Au and Ag, due to their optical properties and chemical stability) and recording the spectra from the solution. The main drawback for this approach is that the uncontrolled aggregation of the NPs may hinder the achievement of a good

reproducibility. Moreover, long term stability issues may appear and not all types of analytes can be mixed with NP suspensions, due to solubility or compatibility issues.[24-25]

For this reason, a great variety of composite materials in which NPs are immobilized on a surface have been proposed to overcome these difficulties. Two main approaches have been used to produce composite SERS substrates: *top-down* methods such as photolithography and nanolithography and *bottom-up* methods, based on the preparation of NPs by colloidal chemistry methods.[25] Lithography techniques allow a fine control over the geometric parameters of the nanostructures, as well as high reproducibility from particle to particle and sample to sample. However, the required setups still have high cost and no mass production is available for the most reproducible structures prepared with these techniques.[24]

Bottom-up approaches, on the other hand, represent a simpler and cost-effective alternative. In this approach, NPs are synthesized by established colloidal methods and then chemically or electrostatically adsorbed on the substrate, typically using bifunctional molecules to obtain covalent bonds or charged polymers to allow electrostatic attachment in a *layer-by-layer* approach.[25] Another possibility in the same direction is the direct production of NPs inside or on the top of the chosen support. Usual supports include glass, metal oxides (such as alumina or quartz), polymers (such as polydimethylsiloxane, poly (vinyl alcohol) or polyamide), hydrogels, metals, silicon wafers, graphene and other 2D materials, and paper.[23-26]

Among all the tested SERS substrates, those based on mesoporous thin films are particularly interesting, since the oxide layer not only provides a support to the NPs but also can be an active part of the sensor.[28-29] The latter feature derives from the fact that mesoporous thin films present a highly ordered array of monodisperse mesopores (diameter of 2 - 10 nm), and a high specific surface area. In addition, their chemical composition can be readily varied from pure to mixed oxides and hybrid organic-inorganic materials.[30-32] In the past, mesoporous thin films and metal NPs had been successfully integrated for SERS applications using different architectures that can be classified in two families, presented in Scheme 1: *(1)* those containing NPs between the substrate and the mesoporous thin film, and *(2)* those in which the NPs are located within the pores or at the walls of the oxide. It should however be mentioned that, a third architecture type has been recently introduced: highly ordered Au NPs deposited on top of mesoporous $SiO_2$ thin films.[33]

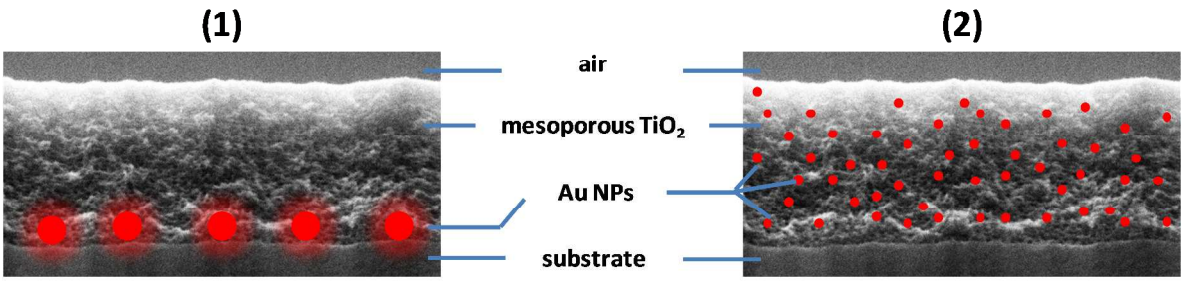


**Scheme 1** Composite architectures involving mesoporous thin films and metal NPs, for SERS applications: *(1)* NPs placed between the substrate and the mesoporous thin film; *(2)* NPs located in the pores or the walls of the oxide.

For architecture *(1)*, Au NPs and $TiO_2$ thin films have been used.[12, 34-35] For architecture *(2)*, combinations of Ag NPs and different mesoporous films ($TiO_2$, $SiO_2$ and $ZrO_2$) have been reported.[36-37] The main features regarding SERS activity and applications of each of these architectures have been presented, though separately and using different measurement conditions. For example, it has been demonstrated that in architecture *(1)* the mesoporous material can be used as a molecular sieve[12, 34] or can provide specificity by modification with a particular chemical function.[35] For architecture *(2)*, on the other hand, it has been demonstrated that the sensors present high signal uniformity, and enhancement factors in the $10^3$-$10^5$ range were proposed.[36-37] However, the SERS community requires standard comparison of SERS substrates, especially when commercial applications are envisioned. In particular, it is highly relevant to have at hand clear information to decide which substrate is most appropriate, depending on the problem to be solved.[38]

In this work, we present a comparative study of the SERS performance of composite materials based on the combination of Au NPs and mesoporous $TiO_2$ thin films, presenting two different general architectures. $TiO_2$ was selected as the mesoporous support material to take advantage of its high chemical and mechanical stability, as well as the open porosity leading to high accessibility of target molecules.[30, 39] Spherical and anisotropic Au NPs of different sizes were used as the plasmonic material due to their good compatibility with the mesoporous synthesis conditions and, especially, for their high chemical stability. The Au NPs were either covered by a mesoporous $TiO_2$ film or synthesized inside the pores of the oxide (Scheme 1). Previously developed architectures were used as a basis to prepare the sensors,[34-35, 40-43] but a wider variety of synthesis conditions were evaluated. Three parameters were chosen to evaluate the sensors' performance, in order to

allow a systematic comparison between the different proposed platforms: minimum acquisition time, spot-to-spot reproducibility and limit of detection (LOD), in all cases using the same standard probe molecule. As some of the proposed applications for this SERS based sensors may require either reproducibility or enhancement to dominate,[20] we propose that the results presented in this work will help understand and establish an objective criterion to select one substrate over another, depending on the envisioned application.[38]

## EXPERIMENTAL SECTION

**Materials.** Tetrachloroauric(III) acid trihydrate ($HAuCl_4 \cdot 3H_2O$), sodium borohydride ($NaBH_4$), (3-aminopropyl)trimethoxysilane (APTES), Pluronic F127 ($HO(CH_2CH_2O)_{106}(CH_2CH(CH_3)-O)_{70}(CH_2CH_2O)_{106}OH$), trisodium citrate dihydrate, cetyltrimethylammonium bromide (CTAB) and ascorbic acid (AA) were purchased from Sigma-Aldrich. Titanium tetrachloride ($TiCl_4$) was supplied by Merck, hydrogen peroxide 28% ($H_2O_2$) by Biopack, sulfuric acid 98% ($H_2SO_4$) by Cicarelli, and para-nitrothiophenol (pNTP) (80%) by Acros-Organics. Phosphate buffer saline (PBS) 0.5 M pH 7.4 was prepared using $Na_2HPO_4$ (Biopack) and $NaH_2PO_4$ (Merck). NaOH and HCl (both Merck) solutions were used to adjust pH when required. All chemicals were used as received. Pure grade ethanol and Milli-Q water were used as solvents.

**Gold nanoparticles synthesis and immobilization.** Citrate-stabilized gold nanospheres of different diameters (15, 35 and 66 nm) were prepared. Nanoparticles of 35 and 66 nm diameter were synthesized according to a previously reported procedure.[44] Briefly, 150 mL of 2.2 mM trisodium citrate was refluxed at 96 °C under vigorous stirring. When the temperature was stabilized, 1 mL of 25 mM $HAuCl_4$ solution was injected into the reaction mixture. After 10 min, the reaction was cooled down to 90 °C. Subsequently, two additions of 1 mL of a 25 mM $HAuCl_4$ aqueous solution were made, separated by 30 minutes. After another 30 min, 55 mL of the obtained solution was extracted and 53 mL of water added with 2.2 mL of 60 mM sodium citrate. The final mixture was used as a seed solution. The whole process with just two injections of the $HAuCl_4$ aqueous solution was repeated again three and seven times to yield 35 nm and 66 nm Au NPs, respectively. 15 nm diameter NPs were obtained using the Turkevich method.[45] Summarily, 250 mL of 0.5 mM $HAuCl_4$ aqueous solution was heated until boiling under vigorous stirring and then 12.5 mL of 38.8 mM trisodium citrate solution was rapidly added. After 20 min of stirring, the reaction was allowed to cool down to room temperature.

Glass slides were immersed in freshly prepared piranha solution (3:1 mixture of $H_2SO_4$ and 30% $H_2O_2$) for 1 hour and then copiously rinsed with pure water. The surface was functionalized by dipping the dry glass slides in a 0.01 M solution of APTES (in pure grade ethanol) for 3 h and then rinsed with ethanol.

Immobilization of Au nanospheres was achieved by immersion of the functionalized glass slides into the gold NPs suspensions (as obtained, without purification) for 20, 40 minutes or overnight (in the latter case, in the fridge). As a result, three different NP densities (*d*) were obtained according to the immobilization time used (*d1* for 20 minutes, *d2* for 40 minutes and *d3* for overnight deposition).

**Mesoporous titania thin film synthesis.** Thin films were produced by either spin-coating or dip-coating**,** taking advantage of the evaporation-induced self-assembly (EISA) strategy using an inorganic precursor ($TiCl_4$) and a template (Pluronic F127) in ethanol.[30] The initial solution was composed of $TiCl_4$/EtOH/F127/$H_2O$ mixture, with a 1:40:0.005:10 molar ratios. This solution was used freshly after preparation.

The films were prepared either over clean glass slides or over the above described Au NP-modified glass slides. In the former case, the deposition was performed by dip coating using a 1 mm $s^{-1}$ speed. The film was removed from one side of the glass slide using an ethanol wetted tissue immediately after deposition. Au NP-modified glass slides, on the other hand, were covered by spin-coating 125 µL of the precursor solution at a spinning speed of 8000 rpm.

Once the films were deposited on the substrates, they were placed in a 50% relative humidity (RH) chamber (obtained with a $Ca(NO_3)_2$ saturated solution) for 24 h and subjected to a stabilizing thermal treatment procedure comprising two successive 24 h heat treatments at 60 and 130 °C, and a final step at 200 °C for 2 h (from 130 °C to 200 °C the temperature was increased using a 1 °C $min^{-1}$ rate). The template was finally eliminated by immersing the films in ethanol for 3 days. Titania films are labeled TF, where F represents the surfactant template F127 used to texture the mesoporous films. Samples in which pre-deposited Au NP were covered by TF films were labeled *Au**X**d**Y**/TF*, where **X** refers to the spherical NPs diameter and **Y** to the NPs density. For example, Au66d2/TF represents a glass slide with 66 nm diameter Au spheres immobilized for 40 minutes and subsequently covered with a TF film.

**Nanoparticle Seeded Growth.** Anisotropic growth of the Au NPs below the mesoporous films was carried out as previously reported.[41] Briefly, the former composite *Au**X**d**Y**/TF* films were immersed in a solution containing $HAuCl_4$, CTAB, and AA with a molar ratio of 1:60:16 ([Au (III)] = $6.25x10^{-5}$

M) for two hours. This procedure, called growth step, was repeated 3 times. After each growth step, the films were rinsed with water and dried in air. The obtained NPs present a shape that resembles a nanostar (NS) and thus were labeled as *Au**NSX**d**Y**/TF*, where **X** refers to the spherical NPs original diameter and **Y** to the NPs density.

**Gold nanoparticles synthesis inside $TiO_2$.** Synthesis of Au NPs inside mesoporous titania thin film was achieved following a reported method.[43] The film was immersed for 1 minute in a 1 mM solution of $HAuCl_4 \cdot 3H_2O$ at pH 4. In these conditions, the adsorption of $AuCl_3(OH)^-$ can occur on the positively charged surface of $TiO_2$. After this time, the film was washed, air dried and dipped for 1 minute in a 5 mM $NaBH_4$ freshly prepared solution, for the reduction of adsorbed Au(III). Finally, the film was rinsed with water. This procedure, called reduction step (RS), was repeated as many times as desired to increase the filling fraction of the mesoporous framework. The samples were labeled *Au**Z**RS@TF*, where **Z** refers to the number of RSs that the film was submitted to. For example, Au5RS@TF refers to a TF film subjected to 5 RSs.

**Characterization.**

***Optical characterization.*** UV−vis−NIR spectra were recorded using a HP Agilent 8453 spectrophotometer or an Ocean Optics spectrophotometer operating with a DH-2000-BAL deuterium and halogen lamps, and a QEPro CCD spectrometer.

***Electron Microscopy.*** Transmission electron microscopy (TEM) analysis was performed by using a Philips CM 200 microscope operating at an acceleration voltage of 180 kV. Samples for TEM were obtained by scratching off the films from the substrate and depositing them on FORMVAR/carbon-coated copper grids. Scanning electron microscopy (SEM) was carried out using a Carl-Zeiss SUPRA 40 microscope. Films for SEM were cut and positioned perpendicular to the holder, so as to observe the NPs placed between the film and the substrate. Energy-dispersive spectroscopy (EDS) was performed in a Philips SEM microscope equipped with an EDAX detector. To carry out this analysis, samples were scratched off from the substrate and deposited on adhesive carbon tape.

***X-ray reflectometry (XRR).*** XRR studies allow us to determine film thickness and porosity, as well as Au loading fraction.[46] Measurements were performed on a Panalytical Empyrean X-Ray diffractometer with an incident beam of Cu $K\alpha_\alpha$ radiation at 1.54 Å, and an incident angle of 1°. A divergence slit of 0.38 mm and a mask of 10 mm were used for the measurements. Film thickness was determined from the Kiessig fringes in the reflectogram. Film porosity was estimated by measuring the shift in the critical angle when the relative humidity (RH) was changed from <5% (i.e. the pores are full of air) to >90% (i.e. the pores are filled with water). Au loading fractions

were calculated measuring the shift in the critical angle at a low humidity (<5%) before and after Au NPs synthesis inside the mesopores. For these purposes, the measurements were made with the films placed inside a controlled humidity chamber. More details about porosity and filling fractions calculations are presented in the Supporting Information.

**SERS experiments and analysis**

***Incubation protocol.*** Film fragments of about 0.5 x 0.5 $cm^2$ were immersed overnight in 1 mL of a pNTP solution (solvent: PBS pH 7.4) in the fridge, then rinsed with water and air-dried. For comparative studies, the concentration of pNTP was $4x10^{-4}$ M. To determine the LOD, solutions were prepared from successive dilutions of the $4x10^{-4}$ M solution. In all cases, pNTP solutions were freshly prepared prior to use.

***Instrumental.*** SERS experiments were recorded with a Horiba LabRAM HR Raman system (Horiba Jobin Yvon) equipped with a Peltier-cooled CCD detector and band-pass filter optics. A 600 grooves $mm^{-1}$ grating was used. A HeNe laser operating at 632.8 nm was chosen as the excitation source, with a power output of 12 mW. All measurements were performed with a confocal microscope in backscattering geometry using a 100x objective with a numerical aperture (NA) value of 0.9. Measurements were carried out in confocality mode with a 100 µm pinhole. Probe degradation at high laser power intensities is common in SERS experiments, thus a 0.1% filter was used to maintain the power at the sample below 5 µW; the filter was selected to keep the probe unaltered during the measurements (see an example of the laser effect over the probe at different powers, in Figure S1).

***Analysis***. Spectra acquisitions were obtained from 8 to 40 points in each sample. Mappings were carried out in 40 x 40 $\mu m^2$ areas (9 points), or 20 x 20 $\mu m^2$ areas (4 points). Accumulation time at each point was varied from 5 s to 120 s (1 scan). For data processing, the 1340 $cm^{-1}$ band, corresponding to the antisymmetric stretching of the nitro group of pNTP, was fitted with a Lorentzian and its intensity was determined for analysis. For comparative studies each sample was characterized by: (1) the minimum acquisition time required to obtain a proper signal-to-noise ratio (S > 3N) in at least 90% of the measured points; (2) intensity spatial distribution; and (3) LOD. For LOD experiments, 10 s and 60 s acquisition times were used. If signal was observed in less than 90% of the points, the concentration was assumed to be less than the detection limit.[47] All the SERS spectra presented here were processed with a smooth function (Savitzky-Golay).

## RESULTS AND DISCUSSION

The comparative study involved the analysis of the SERS performance of different nanoparticle-mesoporous composite designs, comprising the two main architectures depicted in Scheme 1: *(1)* Au NPs placed between the substrate and a titania mesoporous thin film (named *AuXdY/TF* for spherical Au NPs, and *AuNSXdY/TF* for Au nanostars); *(2)* Au NPs located in the porous structure of a titania mesoporous thin film (named: *AuZRS@TF*). Within each architecture, a range of different substrates were designed, which will be discussed in more detail below. Tables 1 and 2 summarize all synthesized samples for architectures *(1)* and *(2)*, respectively.

**Table 1** Description of samples built by architecture *(1)*: Au NPs immobilized between the substrate and the mesoporous film. Anisotropic growth was carried out in these samples.

| NP diameter/nm | immobilization time – NP density | sample name | sample name after anisotropic growth |
|---|---|---|---|
| 15 | 20 min – d1 | Au15d1/TF | AuNS15d1/TF |
| | 40 min – d2 | Au15d2/TF | AuNS15d2/TF |
| | overnight – d3 | Au15d3/TF | AuNS15d3/TF |
| 35 | 20 min – d1 | Au35d1/TF | AuNS35d1/TF |
| | 40 min – d2 | Au35d2/TF | AuNS35d2/TF |
| | overnight – d3 | Au35d3/TF | AuNS35d3/TF |
| 66 | 20 min – d1 | Au66d1/TF | AuNS66d1/TF |
| | 40 min – d2 | Au66d2/TF | AuNS66d2/TF |
| | overnight – d3 | Au66d3/TF | AuNS66d3/TF |

**Table 2** Description of samples built by architecture *(2)*: Au NPs synthesized inside the pores of a mesoporous film.

| number of reduction steps (RS) | sample name |
|---|---|
| 5 | Au5RS@TF |
| 10 | Au10RS@TF |
| 20 | Au20RS@TF |

**Au*X*d*Y*/TF – system characterization.** NPs of different sizes were synthesized, immobilized during different times on APTES-functionalized glass slides and coated with $TiO_2$ mesoporous thin films as described in the experimental section. The $TiO_2$ thin film coating on these substrates had a thickness of 140 nm and a porosity of 45 %, as determined by XRR measurements (see SI for details). These $TiO_2$ films present a pore diameter of ~8 nm, as determined by ellipsometric porosimetry.[48]

Figure 1a shows the UV-visible absorption spectra of the different obtained composites, for the samples containing 66 nm Au NPs (*Au66dY/TF*).

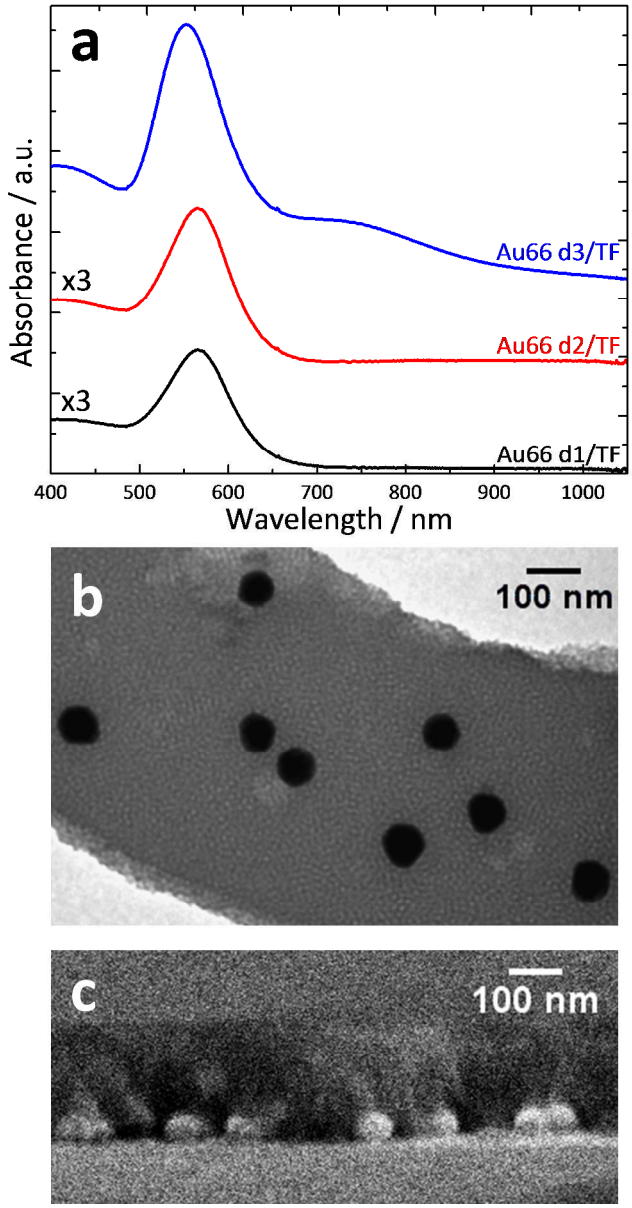

**Figure 1 (a)** UV-visible spectra of *Au66dX/TF* samples with different NP densities, as indicated in the labels **(b)** TEM image of Au66d2/TF. **(c)** SEM image of Au66d3/TF (side-view).

From UV-visible spectra, the first observation is that the intensity of the plasmonic band depends on the incubation time used to attach the Au NPs, determining a density of NPs that can also be quantified using EDS (see Table S2, SI). For low NP densities (d1 and d2), a single narrow LSPR band can be seen, which corresponds to isolated 66 nm diameter NPs covered with mesoporous titania. For longer immobilization times, i.e. higher densities (d3), an increase in the intensity of this band is observed, in agreement with a larger amount of NPs, but also the appearance of a second band above 700 nm, which is attributed to plasmon coupling between NPs localized close to each other within small aggregates. TEM images (Figures 1b, S2b and S3b) confirm that the TF film is porous, with a locally ordered structure and that the Au NPs size and shape remained unaltered upon film deposition and thermal treatment, as previously reported.[41] For low densities, NPs seem to be uniformly distributed throughout the substrate. However, when the NP density is increased, aggregation occurs, as can be seen from the side-view SEM micrographs (Figure 1c). Furthermore, from these images it can be concluded that the mesoporous thin film formation was not affected by the roughness of the substrate imposed by the immobilized NPs.[49] Similar results were obtained for *Au15dY/TF* and *Au35dY/TF* systems (Figures S2 and S3, respectively).

In general, NPs result uniformly distributed on functionalized glass surfaces when short immobilization times are used, but partial aggregation takes place when immobilization time is increased. It is important to highlight that the morphology of the NPs is not affected by film deposition, and the mesoporous film properties are not influenced by the presence of NPs on the substrate.

**AuNS*X*d*Y*/TF – system characterization.** Anisotropic growth of the NPs deposited below the mesoporous film was achieved, as previously reported for similar systems, where the porosity of the $TiO_2$ film acts as a template to guide seeded growth.[34] Throughout the synthesis, a significant change in the film´s color (pink to blue/grey, Figure S4) was identified, which indicated an alteration in the NP morphology. Figure 2a shows the absorbance spectra of the samples with low NP density, before (*AuXd2/TF*) and after anisotropic growth (*AuNSXd2/TF*). In all cases, the spectra after growth display two bands: a lower wavelength band attributed to a dipolar LSPR localized in the NP core and a second band at higher wavelength, attributed to the dipolar plasmon modes localized at the grown tips.[41] TEM images (Figures 2b-d) indeed show that Au nucleation and

growth occurred specifically on the NPs located below the film (which act as seeds) and not at the film walls. Because the growth can only occur through the pores in contact with the seeds, NPs with star/flower-like morphology were obtained. Bigger NPs cores resulted in more extensively branched NPs, *i.e.* with a larger number of tips, because the seeds were in contact with more pores. Moreover, these results indicate that, for all tested cases, the TF film is fully accessible for molecule diffusion from the external solution to the metal NP surface.

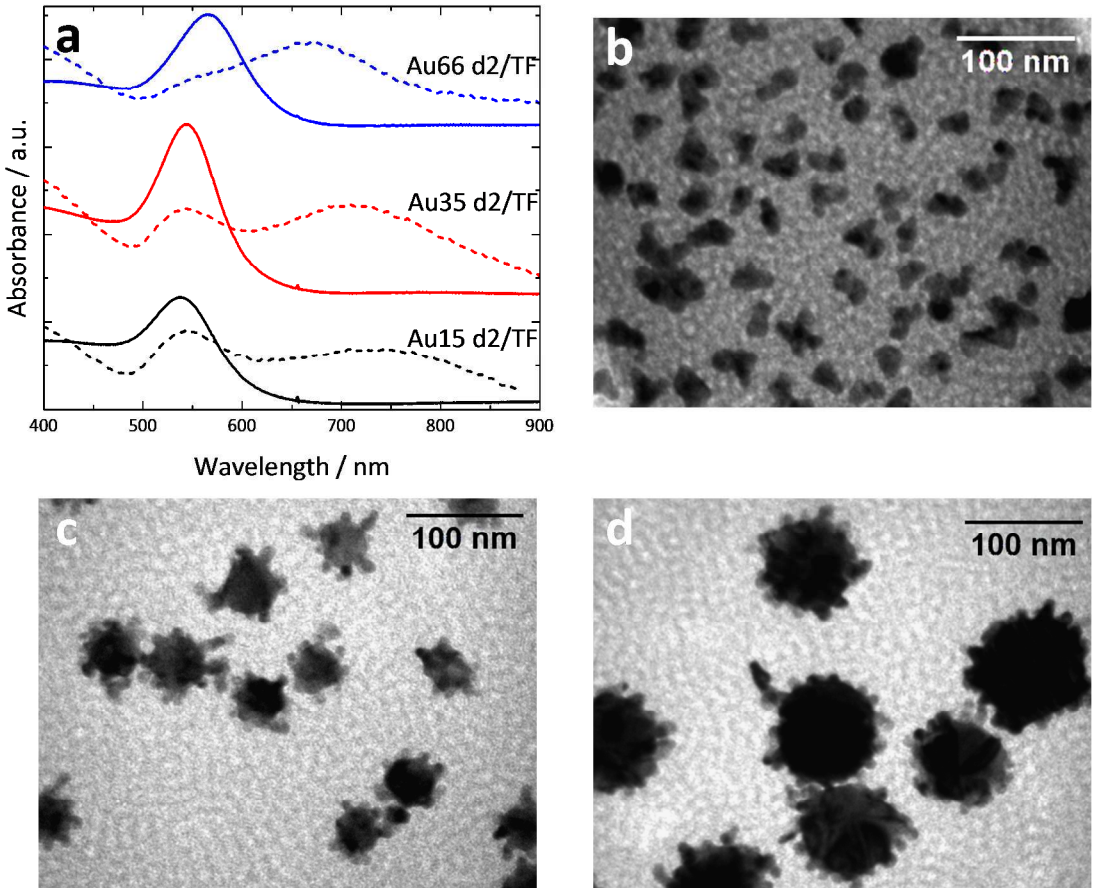


**Figure 2 (a)** UV-visible spectra of *AuXd2/TF* samples before (solid line) and after seeded anisotropic growth (dash line). TEM images of **(b)** AuNS15d2/TF, **(c)** AuNS35d2/TF, and **(d)** AuNS66d2/TF.

**AuZRS@TF – system characterization**. The films used for Au NPs synthesis had a thickness of 160 nm, a pore diameter around 8 nm according to ellipsometric porosimetry [48], and a porosity of 45 %, as determined by XRR. The formation of the NPs inside the mesoporous $TiO_2$ thin film was achieved by repeating the adsorption-reduction process as described above. The first step thus involves the adsorption of $Au^{3+}$ species which are subsequently reduced to Au using $NaBH_4$, in a

second step. Au NP formation proceeds through nucleation and growth. The mechanism has been described in detail in previous works.[42-43] Briefly, during the first synthetic steps fast nucleation occurs, while further exposure to Au(III) precursor and reducing agent leads to concurrent nucleation and growth processes. Visually, as the number of RS was increased, the characteristic uncolored TF film changed into a pink/purple color, typical of spherical Au NPs in a high-index dielectric environment. Moreover, the color intensity increased when the number of RS was increased (Figure S6).

Figure 3a shows the UV-visible spectra of Au NPs-loaded TF after 5, 10 and 20 RS. As a result of nucleation and growth of Au NPs, a well-defined plasmon band gradually develops. The plasmon band maximum was found to red-shift from 540 nm to 556 nm and its intensity increased as the number of RS was incremented. This can be attributed to an increase in both the number of NPs and the NP size. From TEM micrographs (Figure 3b for Au20RS@TF, and Figure S5 for Au10RS@TF and Au5RS@TF) it is clear that NPs, visualized as dark spots, are uniformly distributed inside the mesoporous structure and through the film thickness (Figure S5c). Size analysis revealed that the average NP diameter increased from (5.8 ± 0.7) nm to (9 ± 1) nm when the RS was raised from 5 to 20 (Figure S7). In fact, the particle size could be tuned by the number of RS but was limited by the pore dimensions.[43] The filling process of the mesoporous film was quantitatively monitored by XRR. An increment in the material's critical angle was observed when the number of RS was increased (Figure 3c). This can be directly linked to an increase in material's electronic density, given by the loading of Au NPs into the mesoporous film. The calculated filling fractions are presented in Table S1: 4% of the porosity was occupied when 5 RS were performed and 19% after 20 RS.

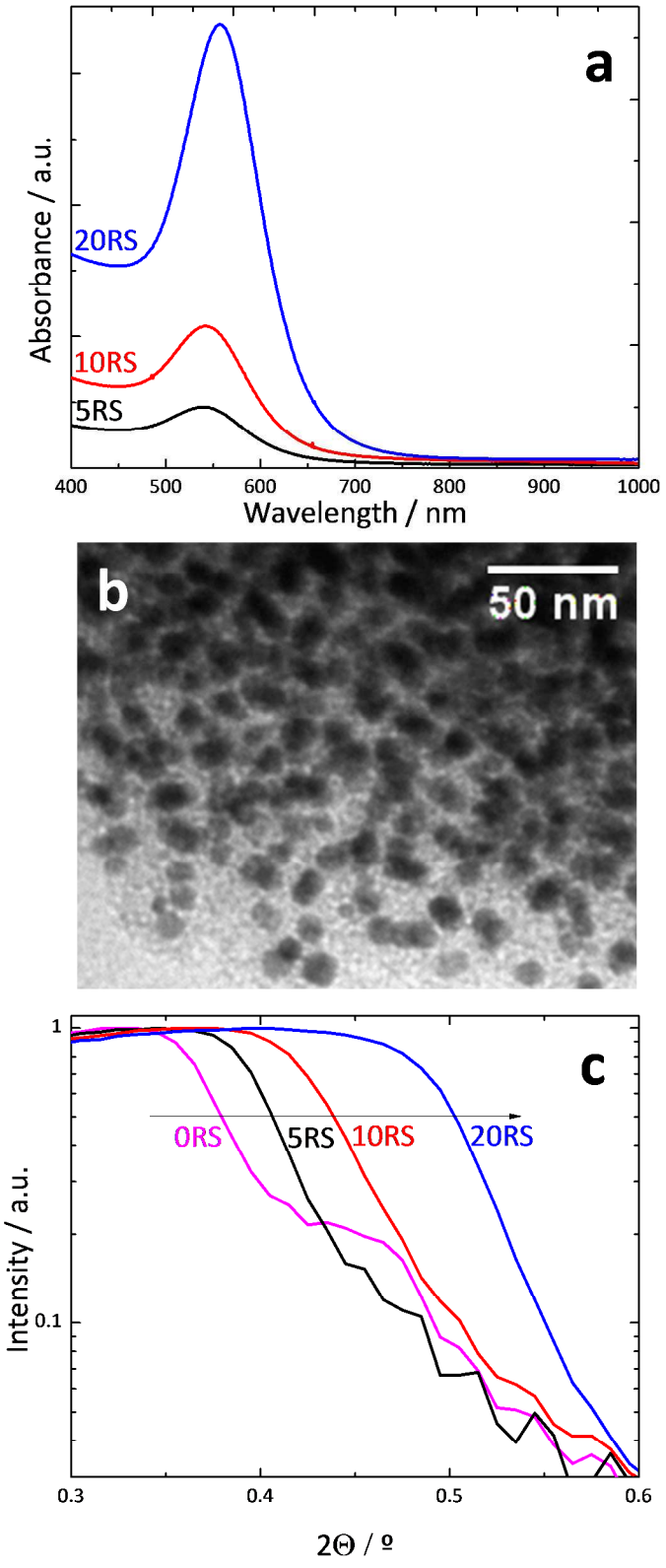


**Figure 3 (a)** UV-visible spectra of *AuZRS@TF* samples (*Z* = 5, 10 and 20) **(b)** TEM image of Au20RS@TF. **(c)** X-Ray Reflectivity data measured at RH<5% for *AuZRS@TF* samples.

**SERS performance.** Comparative SERS studies were performed using pNTP as the probe analyte. This molecule was chosen because it presents a high Raman cross section, binds covalently to Au surfaces and does not possess electronic excited states (or molecular resonances) in the visible region. Upon adsorption on the various hybrid platforms, pNTP SERS spectra were recorded (Figure 4). In all cases, the SERS signals corresponding to the characteristic vibrational bands of pNTP are recognized: C=C stretching (1573 $cm^{-1}$), $NO_2$ symmetric stretching (1340 $cm^{-1}$), and CH bending modes (1083 and 1110 $cm^{-1}$).[50] No major spectral differences were appreciated between measurements from different architectures, thereby ruling out any variation among samples regarding analyte bonding or degradation.

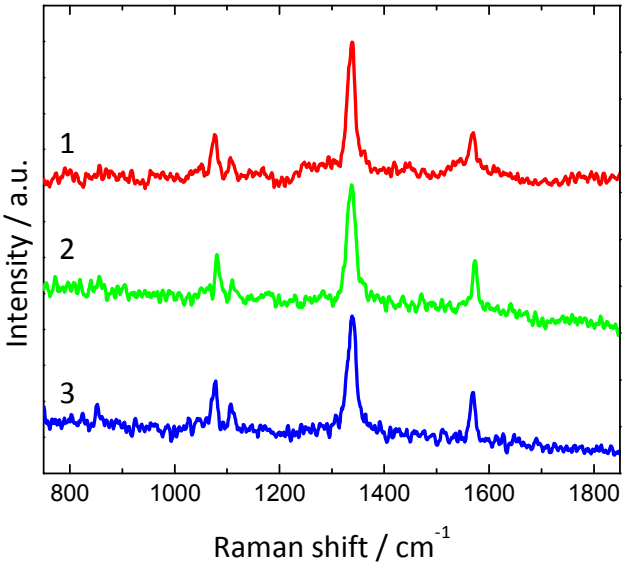


**Figure 4** Normalized pNTP SERS spectra from different platforms: (1) Au66d3/TF, (2) AuNS66d2/TF, and (3) Au20RS@TF.

SERS analysis was carried out using at least 5 replicas for each sample. For this purpose, samples were synthesized and evaluated throughout at least a year. No significant differences in optical or morphological properties neither in SERS performance were observed. The samples are easy to prepare and their synthesis and performance are highly reproducible. Importantly, the selected materials (Au and $TiO_2$) provide the samples with high stability in time, so they could be stocked and used when desired, a clear advantage over substrates prepared using easily oxidizable Ag.[36-37]

The enhacement factor (EF) has been proposed as a useful parameter to compare SERS substrates, particularly for measurements performed in solution. EF calculation requires the use of a reference spectrum, obtained without the presence of the enhancing metallic nanostructure.[3, 24] As the Raman signal of pNTP adsorbed onto a mesoporous $TiO_2$ thin film could not be detected (in agreement with previous results for similar systems[36]), solid pNTP was used as a reference. To calculate the EF, Raman and SERS spectra were recorded for the analyte and the number of molecules contributing to the signal (*n*) in each case was estimated (see SI for details). Since the actual determination of *n* requires to know exactly the amount of free surface area provided by the NPs and the density of the probe molecule adsorbed on the NPs surface,[37] an upper limit for *n* was calculated, yielding a conservative estimate of the EF. As a result, the calculated EF values were in the order of $1x10^5$ for architecture *(1)* (Au66NSd2/TF) and $4x10^2$ for architecture *(2)* (Au20RS@TF). The latter value is two orders of magnitude below the calculated value for similar systems prepared using Ag NPs.[37] However, this is only an approximation that underestimates the SERS enhancing capabilities of the sensors. Therefore, other parameters were chosen to study the potential of the different substrates and to evaluate their performance in a more comprehensive comparative way.

The first parameter proposed for the comparative analysis was the minimum acquisition time required to obtain a suitable signal (S)-to-noise (N) ratio (S > 3 times N) in at least 90% of the measured points, using one scan. The pNTP concentration for these experiments was $4x10^{-4}$ M, so as to ensure that the probe molecule reached the whole metal NP surface, including nanometric gaps between NPs, thereby enabling the study of all the available surface.[51] The obtained results are summarized in Figure 5.

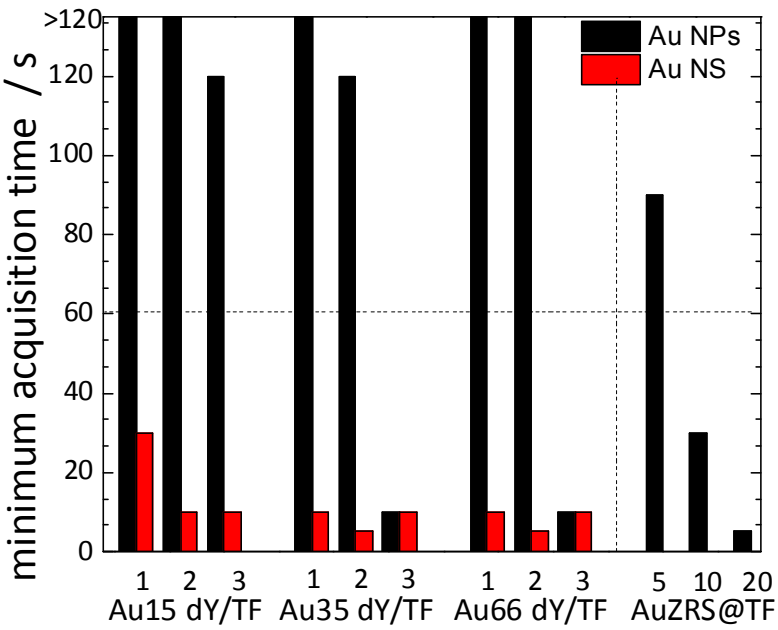


**Figure 5** Minimum acquisition time required for S > 3N. Black bars represent samples prepared with spherical NPs (*AuXdY/TF* and *AuZRS@TF* samples) and red bars represent samples with Au NS (*AuNSXdY/TF* samples).

SERS signal intensity was found to depend linearly on acquisition time (Figure S9, SI), and, although this is not an absolute parameter, a low minimum acquisition time is correlated with a greater SERS sensitivity. In particular, acquisition times below 60 seconds can be considered reasonable for analytical purposes. In this way, two groups can be identified from Figure 5: (a) those samples in which more than 60 s were needed for detection and thus are not useful for analytical applications, and (b) those samples with potential application as SERS sensors because less than 60 s were required for analysis (see dotted horizontal line in Figure 5). This differentiation enables determining the requirements to design a promising SERS sensor based on Au NPs and $TiO_2$ mesoporous films; the relationship between the minimum acquisition time parameter and the structural properties of the systems are discussed below.

For *AuXdY/TF* samples, the minimum acquisition time required to see S > 3N was found to decrease with an increasing NP density. This behavior can be explained considering that a larger metallic surface is available for analyte attachment and, more importantly, there is a greater amount of extrinsic hotspots given by the proximity of the NPs.[19] When NPs are placed close to

each other the electromagnetic field gets further enhanced due to hot spot formation. The highest electromagnetic fields have been found to be generated when the gaps between the curved metallic surfaces are decreased to 1 nm.[52] As a result, at low NP densities (d1 and d2) more than 120 seconds were needed to observe a signal due to the high degree of isolated NPs, whereas at high NP density (d3) and corresponding higher hot spot density, 10 seconds were enough for a reliable detection. As a consequence, only the d3 samples can be considered for further applications.

In addition to NP density, NP size should also be considered. A notable difference was found between those platforms built with the smallest NPs (15 nm diameter) and those with the larger ones (35 and 66 nm diameters). As expected, high acquisition times were needed for 15 nm NPs since they yield a lower electromagnetic enhancement.[53,54] Furthermore, the accessibility of the molecular probe to the surface of these smaller NPs is more hindered since a bigger proportion of the NPs surface is covered with the oxide matrix walls. Thus, this system does not seem useful for analytical applications, in agreement with previously reported results.[34] Finally, no significant differences were observed between those systems built with 35 and 66 nm NPs, when minimum acquisition time was used as the comparative parameter.

For the case of *AuNSXdY/TF* samples (anisotropic NPs), the minimum acquisition time was significantly lower than for equivalent samples *AuXdY/TF* (spherical NPs), as expected from the presence of high electromagnetic fields at the sharp tips resulting from directional growth.[34, 55-56] Additionally, the LSPR red-shift due to branch formation displays a better match with the excitation wavelength. Since both of these facts result in higher SERS enhancements, the sensitivity of the platforms is largely improved and all the *AuNSXdY/TF* samples can be considered as promising sensors. Moreover, *AuNSXd2/TF* samples are more sensitive than *AuNSXd1/TF* samples, which is directly associated with the higher number of NPs with tips per unit area at d2 samples, i.e. a higher number of intrinsic hotspots. For *Au35d3/TF* and *Au66d3/TF* before and after growth, no difference in minimum acquisition time was observed, likely because the close proximity of Au NPs with tips does not lead to significantly better SERS performance.[52]

For *AuZRS@TF* samples, the minimum acquisition time required to obtain S > 3N decreases with increasing Au filling fraction. This observation is attributed to a higher electromagnetic enhancement provided by a reduction in average NP-NP distance, as well as the increase in Au content inside the oxide film and in NP diameter. Similar trends were observed previously for Ag@TF systems with different degrees of Ag NPs filling.[36]

Lastly, it is of interest to compare the performance of isolated NPs deposited below the mesoporous film (*AuXd2/TF)* with that of NPs prepared *in situ* within the film (*AuZRS@TF*). The NPs used for *AuXd2/TF* samples are typically larger than those in *AuZRS@TF* samples, so a greater sensitivity for the first case could be expected. However, the opposite behavior was observed, meaning that this is not the only parameter to be considered. Since mesoporous thin films have a high specific surface, the number of NPs synthesized in *AuZRS@TF* is much larger than those adsorbed on a glass surface prior to film deposition. In fact, EDS measurements (Table S2) show that the amount of Au in *AuXd2/TF* is 2- and 5-fold lower than in samples Au10RS@TF and Au20RS@TF, respectively. Therefore, we can conclude that, for *AuZRS@TF* samples less acquisition time is needed for detection because there is an increase in the available plasmonic enhancing volume that gives rise to hot spots and preconcentration of the analyte. In fact, for Au20RS@TF the minimum acquisition time parameter is comparable to that of high density platforms (Au35d3/TF or Au66d3/TF).

Another critical parameter that must be taken into account when studying the performance of SERS-active substrates is the spatial distribution of the signal. Mappings with a step size of 10 µm were carried out, and the most intense band of pNTP (1340 $cm^{-1}$) was used for analysis. Figure 6 shows the intensity of this band plotted as a function of spatial coordinates for different samples. Displayed in Figure 6a is a map obtained from sample Au66d2/TF (120 s acquisition time), where poor signal or even no signal was recorded. Upon growing tips from Au NPs (AuNS66d2/TF sample - Figure 6b) or increasing NP density (Au66d3/TF sample - Figure 6c), the signal intensity was found to increase, but resulting in a broad inhomogeneity, meaning that the formation of hotspots throughout the substrate was not uniform. On the other hand, the spatial distribution of the signal obtained for samples *AuZRS@TF* was particularly interesting. Figure 6d shows a mapping for pNTP incubated in Au20RS@TF (10 s acquisition time), whilst intensity graphs as a function of spot number are presented in Figure S10. A uniform spatial distribution with a standard deviation below 10% was consistently obtained in all the evaluated probe concentrations above the LOD. In this case, the ordered mesoporous structure functioned as a pattern or matrix where NPs were evenly synthesized and distributed, which is not easy to obtain through soft chemistry.[20] Similar results were previously obtained with Ag NPs synthesized inside mesoporous thin films,[36] but even when Ag NPs give rise to higher SERS enhancements, the use of Au ensures better stability over time.

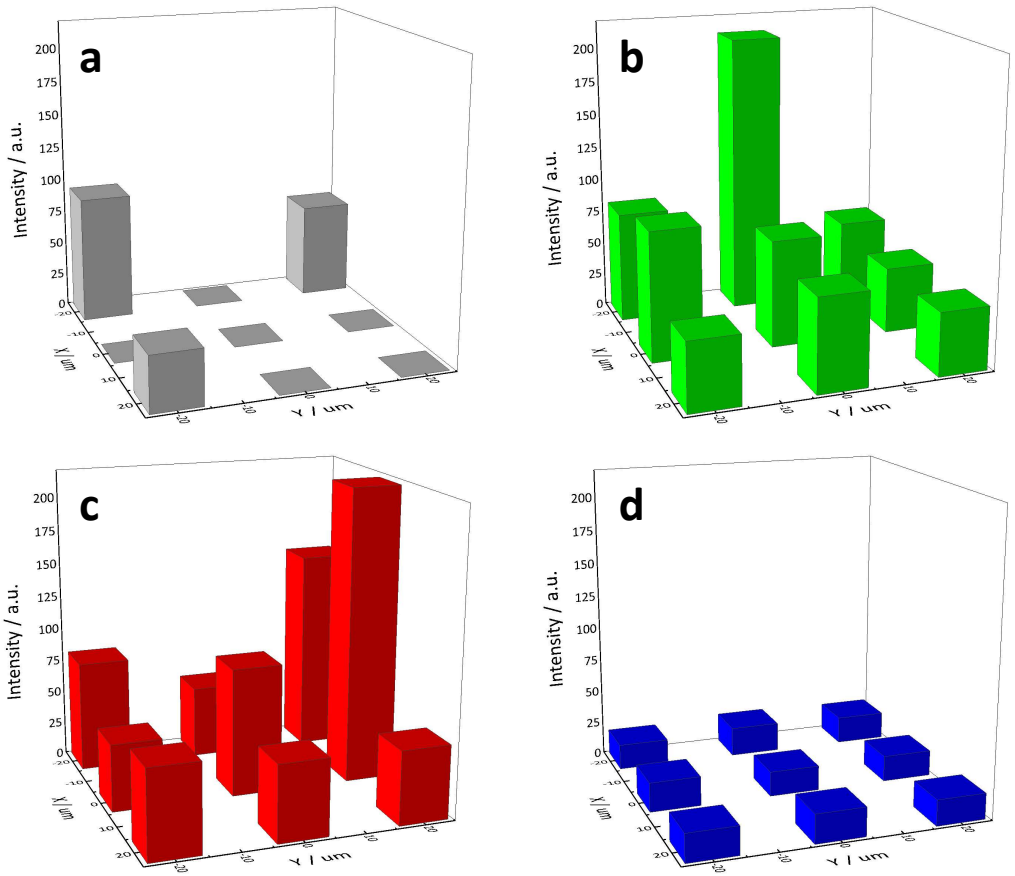


**Figure 6** SERS maps of 1340cm$^{-1}$ band intensity for different samples (pNTP 4 10$^{-4}$ M): (a) Au66d2/TF (120 s acquisition time), (b) AuNS66d2/TF (10 s acquisition time), (c) Au66d3/TF (10 s acquisition time), and (d) Au20RS@TF (10 s acquisition time).

Finally, to complete the understanding of the performance of the SERS platforms, LODs were determined. For this purpose, consecutive dilutions of the pNTP solution were prepared. More than 10 points were evaluated and, in those cases where the signal was only observed in less than 90% of the points, the concentration was assumed to be lower than the detection limit. The obtained results are presented in Figure 7; additional data are presented in Table S4 and Figure S11. Since the future use of these platforms will depend on the specific experiment to be carried out, two different acquisition times were tested: 10 and 60 seconds. However, it is important to note that the presented LODs are the result of the average of different spots in each sample. As a consequence, for inhomogeneous samples the LODs do not present the expected linear relationship with acquisition time (shown in Figure S9).

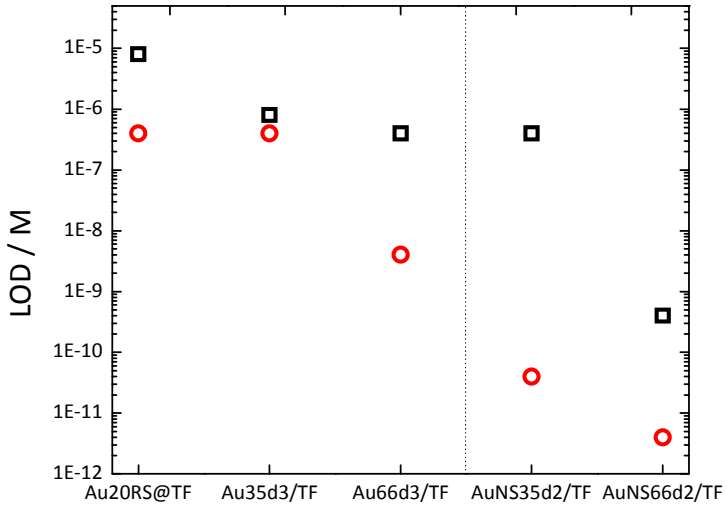


**Figure 7** LOD for selected spherical Au NP and Au NS samples. Squares stand for 10 seconds detection time and circles for 60 seconds detection time.

Detection limits below µM concentration were obtained for the most promising sensors. It is worth mentioning that for samples presented in Figure 7, no significant difference was observed using minimum acquisition time as a performance parameter. However, there are important dissimilitudes regarding the LOD. For the case of *AuXd3/TF* samples, lower LOD were obtained for the larger NPs. As previously mentioned, it is known that the electromagnetic enhancement increases for larger NPs, which is indeed reflected in the obtained LOD. However, a direct comparison of the LOD obtained for *AuXd3/TF* samples with the one obtained for Au20RS@TF sample is difficult, since the latter display smaller NPs but distributed in a different way.

On the other hand, even though a higher sensitivity was achieved by increasing the Au NPs density, the effect of anisotropic growth was more pronounced: the obtained LOD for samples after growth was below that for the samples with high NP density. For AuNS35d2/TF, the LOD of pNTP is in the order of 10 pM, and around 1 pM for AuNS66d2/TF (60 s detection time in both cases), which can be attributed to differences in the number of tips per NP. Therefore it can be concluded that the latter two substrates are optimal for SERS ultradetection.

## SUMMARY AND CONCLUSIONS

Different SERS sensors based on mesoporous $TiO_2$ and Au NPs were prepared, on the basis of previously reported architectures. The density of Au NPs under mesoporous $TiO_2$ was varied for three different particle sizes, and the resulting composites were also compared before and after seeded growth of sharp tips from the Au NPs. As a comparison, mesoporous $TiO_2$ films filled with different amounts of Au NPs within the pores were also developed.

As a general result, it was found that by tuning the different synthetic conditions it is possible to obtain systems that provide a strong SERS signal for pNTP as a molecular probe. Moreover, the chemical characteristics of the components provided all developed platforms with high stability, both in terms of structure and SERS response over time, which is a key point in the development of viable sensors.

All platforms were compared in terms of the minimum acquisition time required to obtain a sufficient signal-to-noise ratio, uniformity of signals' spatial distribution and LOD. Each kind of developed platform displayed different sensing capabilities. Systems containing Au NPs within the pores allow working with low acquisition times, present extremely high signal uniformity, and can reach detection limits in the order of μM. Even though these sensors do not present high enhancements of the Raman signal, they profit from extremely high signal uniformity. Thus, these sensors may find application in routine detection of organic molecules using portable Raman equipment, analytes quantification[57, 58] or catalytic studies.[17, 33] On the other hand, systems composed by overgrown Au NPs covered with mesoporous $TiO_2$ require low acquisition times and can achieve detection limits as low as 10 pM, but present the limitation of lower signal uniformity. These sensors have already demonstrated application for detection in complex media, taking advantage of the filtering ability of mesoporous oxides,[12, 34-35] and their use for ultradetection can also be envisioned. The relative high signal fluctuation might be compensated by averaging a higher number of spots.

In conclusion, careful comparison between SERS sensor materials based on Au NPs and mesoporous thin films should allow interested users to select the most appropriate configuration for each desired application.

## SUPPORTING INFORMATION

Spectra of probe degradation with different laser power intensities. Au15dY/TF, Au35dY/TF and AuZRS@TF systems characterization. XRR data analysis and results. EDS analysis. Enhancement factor calculations. Signal dependence with acquisition time. SERS signal spatial distribution for AuZRS@TF samples. pNTP limits of detection with SERS spectra.

## ACKNOWLEDGEMENTS

This work has been funded by CONICET (PIP 00044CO) and ANPCyT (PICT 2012-0111, PICT 2012-2087, PICT 2015-3526 and PICT 2015-0351).

We thank Gonzalo Zbihlei for TEM measurements and Mariana Rosenbusch for EDS measurements. J.J.G.-C. acknowledges the Ministry of Economy and Competitiveness for a Ramon y Cajal contract (#RyC-2014-14956). M. M. Z. acknowledges CONICET for a doctoral scholarship.

## REFERENCES

1. Fleischmann, M.; Hendra, P. J.; McQuillan, A. J., Raman spectra of pyridine adsorbed at a silver electrode. *Chem. Phys. Lett.* **1974,** *26* (2), 163-166.
2. Jeanmaire, D. L.; Van Duyne, R. P., Surface Raman spectroelectrochemistry. *Journal of Electroanalytical Chemistry and Interfacial Electrochemistry* **1977,** *84* (1), 1-20.
3. Schlücker, S., Surface-Enhanced Raman Spectroscopy: Concepts and Chemical Applications. *Angew. Chem. Int. Ed.* **2014,** *53* (19), 4756-4795.
4. Kneipp, K.; Wang, Y.; Kneipp, H.; Perelman, L. T.; Itzkan, I.; Dasari, R. R.; Feld, M. S., Single molecule detection using surface-enhanced Raman scattering (SERS). *Phys. Rev. Lett.* **1997,** *78* (9), 1667.
5. Nie, S.; Emory, S. R., Probing Single Molecules and Single Nanoparticles by Surface-Enhanced Raman Scattering. *Science* **1997,** *275* (5303), 1102-1106.
6. Zrimsek, A. B.; Chiang, N.; Mattei, M.; Zaleski, S.; McAnally, M. O.; Chapman, C. T.; Henry, A.-I.; Schatz, G. C.; Van Duyne, R. P., Single-Molecule Chemistry with Surface- and Tip-Enhanced Raman Spectroscopy. *Chem. Rev.* **2017,** *117* (11), 7583-7613.
7. Alvarez-Puebla, R. A.; Liz-Marzán, L. M., SERS Detection of Small Inorganic Molecules and Ions. *Angew. Chem. Int. Ed.* **2012,** *51* (45), 11214-11223.
8. Cho, I.-H.; Radadia, A. D.; Farrokhzad, K.; Ximenes, E.; Bae, E.; Singh, A. K.; Oliver, H.; Ladisch, M.; Bhunia, A.; Applegate, B.; Mauer, L.; Bashir, R.; Irudayaraj, J., Nano/Micro and Spectroscopic Approaches to Food Pathogen Detection. *Annu. Rev. Anal. Chem.* **2014,** *7* (1), 65-88.
9. Álvarez-Puebla, R. A.; Liz-Marzán, L. M., Environmental applications of plasmon assisted Raman scattering. *Energy Environ. Sci.* **2010,** *3* (8), 1011-1017.

10. Álvarez-Puebla, R. A.; Liz-Marzán, L. M., SERS-Based Diagnosis and Biodetection. *Small* **2010,** *6* (5), 604-610.
11. Cialla-May, D.; Zheng, X. S.; Weber, K.; Popp, J., Recent progress in surface-enhanced Raman spectroscopy for biological and biomedical applications: from cells to clinics. *Chem. Soc. Rev.* **2017,** *46* (13), 3945-3961.
12. Bodelón, G.; Montes-García, V.; López-Puente, V.; Hill, E. H.; Hamon, C.; Sanz-Ortiz, M. N.; Rodal-Cedeira, S.; Costas, C.; Celiksoy, S.; Perez-Juste, I.; Scarabelli, L.; La Porta, A.; Pérez-Juste, J.; Pastoriza-Santos, I.; Liz-Marzán, L. M., Detection and imaging of quorum sensing in Pseudomonas aeruginosa biofilm communities by surface-enhanced resonance Raman scattering. *Nat. Mater.* **2016,** *15* (11), 1203-1211.
13. Bodelón, G.; Montes-García, V.; Costas, C.; Pérez-Juste, I.; Pérez-Juste, J.; Pastoriza-Santos, I.; Liz-Marzán, L. M., Imaging Bacterial Interspecies Chemical Interactions by Surface-Enhanced Raman Scattering. *ACS Nano* **2017,** *11* (5), 4631-4640.
14. Costas, C.; López-Puente, V.; Bodelón, G.; González-Bello, C.; Pérez-Juste, J.; Pastoriza-Santos, I.; Liz-Marzán, L. M., Using Surface Enhanced Raman Scattering to Analyze the Interactions of Protein Receptors with Bacterial Quorum Sensing Modulators. *ACS Nano* **2015,** *9* (5), 5567-5576.
15. Xie, W.; Schlücker, S., Medical applications of surface-enhanced Raman scattering. *Phys. Chem. Chem. Phys.* **2013,** *15* (15), 5329-5344.
16. Kurouski, D.; Van Duyne, R. P.; Lednev, I. K., Exploring the structure and formation mechanism of amyloid fibrils by Raman spectroscopy: a review. *Analyst* **2015,** *140* (15), 4967-4980.
17. Cardinal, M. F.; Vander Ende, E.; Hackler, R. A.; McAnally, M. O.; Stair, P. C.; Schatz, G. C.; Van Duyne, R. P., Expanding applications of SERS through versatile nanomaterials engineering. *Chem. Soc. Rev.* **2017,** *46* (13), 3886-3903.
18. Ding, S.-Y.; Yi, J.; Li, J.-F.; Ren, B.; Wu, D.-Y.; Panneerselvam, R.; Tian, Z.-Q., Nanostructure-based plasmon-enhanced Raman spectroscopy for surface analysis of materials. *Nat. Rev. Mater.* **2016,** *1*, 16021.
19. Reguera, J.; Langer, J.; Jimenez de Aberasturi, D.; Liz-Marzán, L. M., Anisotropic metal nanoparticles for surface enhanced Raman scattering. *Chem. Soc. Rev.* **2017,** *46*, 3866-3885
20. Brown, R. J. C.; Milton, M. J. T., Nanostructures and nanostructured substrates for surface—enhanced Raman scattering (SERS). *J. Raman Spectrosc.* **2008,** *39* (10), 1313-1326.
21. Moskovits, M., Surface-enhanced Raman spectroscopy: a brief retrospective. *J. Raman Spectrosc.* **2005,** *36* (6-7), 485-496.
22. Álvarez-Puebla, R.; Liz-Marzán, L. M.; García de Abajo, F. J., Light Concentration at the Nanometer Scale. *J. Phys. Chem. Lett.* **2010,** *1* (16), 2428-2434.
23. Betz, J. F.; Yu, W. W.; Cheng, Y.; White, I. M.; Rubloff, G. W., Simple SERS substrates: powerful, portable, and full of potential. *Phys. Chem. Chem. Phys.* **2014,** *16* (6), 2224-2239.
24. Fan, M.; Andrade, G. F. S.; Brolo, A. G., A review on the fabrication of substrates for surface enhanced Raman spectroscopy and their applications in analytical chemistry. *Anal. Chim. Acta* **2011,** *693* (1), 7-25.
25. Shiohara, A.; Wang, Y.; Liz-Marzán, L. M., Recent approaches toward creation of hot spots for SERS detection. *Journal of Photochemistry and Photobiology C: Photochemistry Reviews* **2014,** *21*, 2-25.
26. Ouyang, L.; Ren, W.; Zhu, L.; Irudayaraj, J., Prosperity to challenges: recent approaches in SERS substrate fabrication. *Rev. Anal. Chem* **2017,** *36* (1).
27. Langer, J.; Novikov, S. M.; Liz-Marzán, L. M., Sensing using plasmonic nanostructures and nanoparticles. *Nanotechnology* **2015,** *26* (32), 322001.

28. Angelomé, P. C.; Fuertes, M. C., Metal Nanoparticles-Mesoporous Oxide Nanocomposite Thin Films. In *Handbook of Sol-Gel Science and Technology*, Klein, L.; Aparicio, M.; Jitianu, A., Eds. Springer International Publishing: Cham, 2016; pp in press, DOI 10.1007/978-3-319-19454-7_146-1.
29. Angelomé, P. C.; Liz-Marzán, L. M., Synthesis and applications of mesoporous nanocomposites containing metal nanoparticles. *J. Sol-Gel Sci. Technol.* **2014,** *70* (2), 180-190.
30. Soler-Illia, G. J. A. A.; Angelomé, P. C.; Fuertes, M. C.; Grosso, D.; Boissiere, C., Critical aspects in the production of periodically ordered mesoporous titania thin films. *Nanoscale* **2012,** *4* (8), 2549-2566.
31. Nicole, L.; Boissiere, C.; Grosso, D.; Quach, A.; Sanchez, C., Mesostructured hybrid organic-inorganic thin films. *J. Mater. Chem.* **2005,** *15* (35-36), 3598-3627.
32. Innocenzi, P.; Malfatti, L., Mesoporous thin films: properties and applications. *Chem. Soc. Rev.* **2013,** *42* (9), 4198-4216.
33. Wang, Y.-W.; Kao, K.-C.; Wang, J.-K.; Mou, C.-Y., Large-Scale Uniform Two-Dimensional Hexagonal Arrays of Gold Nanoparticles Templated from Mesoporous Silica Film for Surface-Enhanced Raman Spectroscopy. *J. Phys. Chem. C* **2016,** *120* (42), 24382-24388.
34. López-Puente, V.; Abalde-Cela, S.; Angelomé, P. C.; Alvarez-Puebla, R. A.; Liz-Marzán, L. M., Plasmonic Mesoporous Composites as Molecular Sieves for SERS Detection. *J. Phys. Chem. Letters* **2013,** *4* (16), 2715-2720.
35. López-Puente, V.; Angelomé, P. C.; Soler-Illia, G. J. A. A.; Liz-Marzán, L. M., Selective SERS Sensing Modulated by Functionalized Mesoporous Films. *ACS Appl. Mater. Interfaces* **2015,** *7* (46), 25633-25640.
36. Wolosiuk, A.; Tognalli, N. G.; Martínez, E. D.; Granada, M.; Fuertes, M. C.; Troiani, H.; Bilmes, S. A.; Fainstein, A.; Soler-Illia, G. J. A. A., Silver Nanoparticle-Mesoporous Oxide Nanocomposite Thin Films: A Platform for Spatially Homogeneous SERS-Active Substrates with Enhanced Stability. *ACS Appl. Mater. Interfaces* **2014,** *6* (7), 5263-5272.
37. Malfatti, L.; Falcaro, P.; Marmiroli, B.; Amenitsch, H.; Piccinini, M.; Falqui, A.; Innocenzi, P., Nanocomposite mesoporous ordered films for lab-on-chip intrinsic surface enhanced Raman scattering detection. *Nanoscale* **2011,** *3* (9), 3760-3766.
38. Natan, M. J., Concluding Remarks Surface enhanced Raman scattering. *Faraday Discuss.* **2006,** *132* (0), 321-328.
39. Bass, J. D.; Grosso, D.; Boissiere, C.; Belamie, E.; Coradin, T.; Sanchez, C., Stability of Mesoporous Oxide and Mixed Metal Oxide Materials under Biologically Relevant Conditions. *Chem. Mater.* **2007,** *19* (17), 4349-4356.
40. Angelomé, P. C.; Liz-Marzán, L. M., Monitoring Solvent Evaporation from Thin Films by Localized Surface Plasmon Resonance Shifts. *J. Phys. Chem. C* **2010,** *114* (43), 18379-18383.
41. Angelomé, P. C.; Pastoriza-Santos, I.; Pérez Juste, J.; Rodríguez-González, B.; Zelcer, A.; Soler-Illia, G. J. A. A.; Liz Marzán, L. M., Growth and Branching of Gold Nanoparticles Through Mesoporous Silica Thin Films. *Nanoscale* **2012,** *4*, 931-939.
42. Martínez, E. D.; Boissière, C.; Grosso, D.; Sanchez, C.; Troiani, H.; Soler-Illia, G. J. A. A., Confinement-Induced Growth of Au Nanoparticles Entrapped in Mesoporous TiO2 Thin Films Evidenced by in Situ Thermo-Ellipsometry. *J. Phys. Chem. C* **2014,** *118* (24), 13137-13151.
43. Sánchez, V. M.; Martínez, E. D.; Martínez Ricci, M. L.; Troiani, H.; Soler-Illia, G. J. A. A., Optical Properties of Au Nanoparticles Included in Mesoporous TiO2 Thin Films: A Dual Experimental and Modeling Study. *J. Phys. Chem. C* **2013,** *117* (14), 7246-7259.
44. Bastús, N. G.; Comenge, J.; Puntes, V., Kinetically Controlled Seeded Growth Synthesis of Citrate-Stabilized Gold Nanoparticles of up to 200 nm: Size Focusing versus Ostwald Ripening. *Langmuir* **2011,** *27* (17), 11098-11105.

45. Turkevich, J.; Stevenson, P. C.; Hillier, J., A study of the nucleation and growth processes in the synthesis of colloidal gold. *Discussions of the Faraday Society* **1951,** *11*, 55-75.
46. Fuertes, M. C.; Marchena, M.; Marchi, M. C.; Wolosiuk, A.; Soler-Illia, G. J. A. A., Controlled Deposition of Silver Nanoparticles in Mesoporous Single- or Multilayer Thin Films: From Tuned Pore Filling to Selective Spatial Location of Nanometric Objects. *Small* **2009,** *5* (2), 272-280.
47. Norrod, K. L.; Sudnik, L. M.; Rousell, D.; Rowlen, K. L., Quantitative Comparison of Five SERS Substrates: Sensitivity and Limit of Detection. *Appl. Spectrosc.* **1997,** *51* (7), 994-1001.
48. Angiolini, J. F.; Stortz, M.; Steinberg, P. Y.; Mocskos, E.; Bruno, L.; Soler-Illia, G.; Angelomé, P. C.; Wolosiuk, A.; Levi, V., Diffusion of single dye molecules in hydrated TiO2 mesoporous films. *Phys. Chem. Chem. Phys.* **2017,** *19* (39), 26540-26544.
49. Rodríguez-Fernández, D.; Angelomé, P. C.; Soler-Illia, G. J. A. A.; Liz-Marzán, L. M. C., Multilayered Materials Comprising Mesoporous Thin Films and Metal Nanoparticles. *Part. Part. Syst. Char.* **2017,** *34* (5), 1600428.
50. Skadtchenko, B.; Aroca, R., Surface-enhanced Raman scattering of p-nitrothiophenol: Molecular vibrations of its silver salt and the surface complex formed on silver islands and colloids. *Spectrochimica Acta Part A: Molecular and Biomolecular Spectroscopy* **2001,** *57* (5), 1009-1016.
51. Novara, C.; Dalla Marta, S.; Virga, A.; Lamberti, A.; Angelini, A.; Chiadò, A.; Rivolo, P.; Geobaldo, F.; Sergo, V.; Bonifacio, A.; Giorgis, F., SERS-Active Ag Nanoparticles on Porous Silicon and PDMS Substrates: A Comparative Study of Uniformity and Raman Efficiency. *J. Phys. Chem. C* **2016,** *120* (30), 16946-16953.
52. Solís, D. M.; Taboada, J. M.; Obelleiro, F.; Liz-Marzán, L. M.; García de Abajo, F. J., Optimization of Nanoparticle-Based SERS Substrates through Large-Scale Realistic Simulations. *ACS Photonics* **2017,** *4* (2), 329-337.
53. Njoki, P. N.; Lim, I. I. S.; Mott, D.; Park, H.-Y.; Khan, B.; Mishra, S.; Sujakumar, R.; Luo, J.; Zhong, C.-J., Size Correlation of Optical and Spectroscopic Properties for Gold Nanoparticles. *J. Phys. Chem. C* **2007,** *111* (40), 14664-14669.
54. Hong, S.; Li, X., Optimal size of gold nanoparticles for surface-enhanced raman spectroscopy under different conditions. *J. Nanomaterials* **2013,** *2013*, 49-49.
55. Guerrero-Martínez, A.; Barbosa, S.; Pastoriza-Santos, I.; Liz-Marzán, L. M., Nanostars shine bright for you: Colloidal synthesis, properties and applications of branched metallic nanoparticles. *Curr. Opin. Colloid Interface Sci.* **2011,** *16* (2), 118-127.
56. Aldeanueva-Potel, P.; Carbó-Argibay, E.; Pazos-Pérez, N.; Barbosa, S.; Pastoriza-Santos, I.; Alvarez-Puebla, R. A.; Liz-Marzán, L. M., Spiked Gold Beads as Substrates for Single-Particle SERS. *ChemPhysChem* **2012,** *13* (10), 2561-2565.
57. Bell, S. E. J.; Sirimuthu, N. M. S., Quantitative surface-enhanced Raman spectroscopy. *Chem. Soc. Rev.* **2008,** *37* (5), 1012-1024.
58. Reyer, A.; Prinz, A.; Giancristofaro, S.; Schneider, J.; Bertoldo Menezes, D.; Zickler, G.; Bourret, G. R.; Musso, M. E., Investigation of Mass-Produced Substrates for Reproducible Surface-Enhanced Raman Scattering Measurements over Large Areas. *ACS Appl. Mater. Interfaces* **2017,** *9* (30), 25445-25454.